RESEARCH ARTICLE

Three-dimensional analysis of the fast-start escape response of the least killifish, *Heterandria formosa*

Mike Fleuren, Johan L. van Leeuwen*, Elsa M. Quicazan-Rubio, Remco P. M. Pieters, Bart J. A. Pollux and Cees J. Voesenek

ABSTRACT

Fish make C-starts to evade predator strikes. Double-bend (DB) C-starts consist of three stages: Stage 1, in which the fish rapidly bends into a C-shape; Stage 2, in which the fish bends in the opposite direction; and a variable Stage 3. In single-bend (SB) C-starts, the fish immediately straightens after Stage 1. Despite fish moving in three-dimensional (3D) space, fast-start responses of adult fish have mainly been studied in a horizontal plane. Using automated 3D tracking of multi-camera high-speed video sequences, we show that both SB and DB fast-starts by adult female least killifish (*Heterandria formosa*) often contain a significant vertical velocity component, and large changes in pitch (DB up to 43 deg) and roll (DB up to 77 deg) angles. Upwards and downwards elevation changes are correlated with changes in pitch angle of the head; movement in the horizontal plane is correlated with changes in yaw angle of the head. With respect to the stimulus, escape heading correlates with the elevation of the fish at the onset of motion. Irrespective of the initial orientation, fish can escape in any horizontal direction. In many cases, the centre of mass barely accelerates during Stage 1. However, it does accelerate in the final direction of the escape in other instances, indicating that Stage 1 can serve a propulsive role in addition to its preparatory role for Stage 2. Our findings highlight the importance of large-scale 3D analyses of fast-start manoeuvres of adult fish in uncovering the versatility of fish escape repertoire.

INTRODUCTION

Fast-start responses are a pivotal manoeuvre in predator–prey interactions of fish: prey exhibit this behaviour to propel themselves away from danger, while predators use it to lunge themselves towards prey (Domenici and Blake, 1997). Similar kinematic patterns have also been observed during other behaviours, including social interactions (Fernald, 1975), following food capture (Canfield and Rose, 1993; Canfield, 2007; Wöhl and Schuster, 2007; Krupczynski and Schuster, 2008) and following air–surface interactions (Domenici et al., 2014).

Fast-start responses can be divided in two types based on their muscle activation and contraction pattern: location-shifted bilateral contraction of the axial muscles results in 'S-starts', named after the S-shaped body bend (Webb, 1976; Spierts and Van Leeuwen, 1999; Hale, 2002), and 'C-starts' that initially follow unilateral muscle contraction, named after the C-shaped body bend (Eaton et al., 1977; Domenici and Blake, 1991, 1997). C-starts are typically described following three distinct stages (Weihs, 1973). During 'Stage 1' the fish bends into the characteristic C-shape, while during 'Stage 2' a contralateral movement of the tail propels the fish away from its original position. C-starts do not by definition have a Stage 2: starts without a Stage 2 are often referred to as single-bend (SB) responses, while starts with a Stage 2 are referred to as double-bend (DB) responses (Domenici and Blake, 1991, 1993a). The last stage, 'Stage 3', is highly variable and can consist of a wide range of motions from continued swimming to gliding or braking with the pectoral fins. Hereafter, we will use the term 'fast start' as a synonym for 'C-start' for the purposes of readability.

Over the past decade, the hypothesized roles of the different stages of the fast start have gradually been changing. Traditionally, Stage 1 and Stage 2 of the fast start have been described as the 'preparatory phase' and 'propulsive phase', respectively (Weihs, 1973). Indicative of the presumed preparatory nature of the first stage, is that the reorientation of the head during Stage 1 is an important determinant for heading of the escape during subsequent stages (Domenici and Blake, 1993b), while forward motion of the head is limited. However, during the C-bend one of the jets propelling the fish is formed (Tytell and Lauder, 2008), and other studies describe significant production of force (Borazjani et al., 2012), or movement and acceleration of the centre of mass (COM) during this stage (Weihs, 1973; Wakeling and Johnston, 1998). Arguably, the term 'preparatory phase' is too narrow and both stages of the fast start may contribute to forward propulsion (Wakeling, 2006).

Multiple methods have been developed to determine the end of Stage 1 and the beginning of Stage 2. Physiologically, it can be determined from the onset of the contralateral electromyography (EMG) signal (e.g. Jayne and Lauder, 1993; Ellerby and Altringham, 2001), but EMG signals during free swimming are generally not available in kinematics studies. From a biomechanical and/or kinematics perspective, different parameters have been used to describe the transition from Stage 1 to Stage 2: the onset of forward propulsion (e.g. Foreman and Eaton, 1993), the change in turning direction of the head or anterior body midline (e.g. Domenici and Blake, 1991; Domenici and Blake, 1993a,b; Kasapi et al., 1993; Spierts and Van Leeuwen, 1999; Goldbogen et al., 2005), or the onset of the return tail beat (e.g. Kawabata et al., 2016). In this paper, we use a novel method to determine the transition between stages with the moment of inertia in the yaw plane, which reflects whole-body kinematics. The differences between these methods result in (slight) deviations in the timing of the several stages and, because of this, in differences in measured parameters at stage-related time points.

Experimental Zoology Group, Department of Animal Sciences, Wageningen University & Research, Wageningen 6708 WD, The Netherlands.

*Author for correspondence (johan.vanleeuwen@wur.nl)

M.F., 0000-0002-3186-3840; J.L.v.L., 0000-0002-4433-880X; E.M.Q.-R., 0000-0002-7320-8924; C.J.V., 0000-0002-5467-8963

Although fish swim in a three-dimensional (3D) space and use the water column as such, fast starts have been often simplified as a 2D manoeuvre with motions parallel to the horizontal plane (Domenici and Blake, 1997). Recently, it was shown that escape responses of larval zebrafish (*Danio rerio*) often contain a considerable 3D component: pitch angle changes of the head correlate with changes in elevation (Stewart et al., 2013; Nair et al., 2015). In two instances, 3D fast-start manoeuvres were reported for adult fish, namely in knifefish (*Pterophyllum eimekei*) and hatchetfish (*Carnegiella strigata*) (Eaton et al., 1977; Kasapi et al., 1993), but fast starts of adult fish are generally reduced to 2D manoeuvres in the literature (e.g. Domenici and Blake, 1997).

The increasing knowledge of the 3D components of fast-start responses follows recent methodological developments. Within the field of fish swimming biomechanics, high-speed video imaging is shifting from 2D to 3D recording with multiple synchronized cameras, and simultaneous advances in automated image analysis allow for processing of large sets of movies (e.g. Voesenek et al., 2016). Most previous work on fast-start responses recorded movement solely in the horizontal plane, with a set-up in which vertical displacement is restricted, and/or discarded movies in which the fish swims out of focus (e.g. Domenici and Blake, 1993a,b; Müller and Van Leeuwen, 2004; Kawabata et al., 2016), while the number of studies that report 3D descriptions of the fast-start response remained limited (Eaton et al., 1977: one documented fast-start response; Kasapi et al., 1993: 14 fast starts). Currently, 3D imaging and analysis is becoming the standard to study swimming kinematics (Butail and Paley, 2012; Nair et al., 2015; Voesenek et al., 2016, 2018).

A second methodological development is the switch from the usage of a fixed point on the body as an estimate for COM (e.g. Spierts and Van Leeuwen, 1999; Lefrançois et al., 2005; Nair et al., 2015), to a dynamic COM that shifts position relative to the body during swimming (2D approach: Wakeling and Johnston, 1998; van Leeuwen et al., 2015; 3D approach: Voesenek et al., 2016). Such a dynamic COM is calculated from the mass distribution along the body, and can lie outside of the fish's body for large body curvatures. From a biomechanical perspective, this results in a more accurate depiction of the motion of the COM during a fast-start manoeuvre compared with the use of a fixed point on the body as a proxy of the COM.

Combining these recent advances from the fields of swimming kinematics and biomechanics, we explore in this study the 3D kinematics of the fast-start escape response of adult least killifish, *Heterandria formosa*. We hypothesize that, similar to the 3D kinematics of the C-start of the larval zebrafish (Nair et al., 2015), yawing and pitching motions of the head are associated with changes in azimuth and elevation, respectively. In addition, we revisit the role of Stage 1 in the fast start, and analyse the 3D escape trajectory relative to the direction of the stimulus source.

MATERIALS AND METHODS
Experimental animals
Experiments were performed with adult females of least killifish (*Heterandria formosa* Girard 1859), a species of the live-bearing fish family Poeciliidae that naturally populates a diversity of habitats in the southeastern USA, including small freshwater lakes, streams and marshes (MacRae and Travis, 2014). Newborn fish from the same age cohort (2–3 weeks) were raised together. Males were removed from these cohorts as soon as secondary sex characteristics started to develop, resulting in all-virgin laboratory populations. Average standard length (L_{sl}) of the experimental animals (N=14)

was 27.57±0.35 mm (mean±s.e.m.). Starting one to two months preceding the experiments, the fish were housed individually at 24°C in 9 l tanks (Tecniplast, Bugugiatte, Italy) that contained a plastic plant, and were fed fixed quantities of flake paste and liver paste (0.05 ml) and approximately five adult brine shrimp in the afternoon after experiments. The experimental fish were subjected to escape response measurements daily: on average, fish were subjected to 8.5 measurement days (range: 5–12 days). All procedures described were approved by the Animal Ethics Committee of Wageningen University & Research (permit number 2013103).

### Escape response measurements
Escape responses were recorded in a 0.23×0.23×0.30 m (length×width×height) aquarium with the water level at 0.23 m (Fig. 1A). Water (23.8±0.3°C; mean±s.d.) was refreshed before introduction of each new individual. The central area of the aquarium (field of view approximately 0.10×0.10×0.10 m) was filmed using three Mikroton EoSens CL MC1362 high-speed video cameras (Mikrotron, Unterschleissheim, Germany; resolution 1040×1020 pixels; 1/1000 s shutter speed) equipped with Voigtländer Ultron F=40 mm 1:2 aspherical compact pancake lenses (RINGFOTO, Fürth, Germany) and Epix PIXCI E8 frame grabbers (EPIX, Buffalo Grove, IL, USA). A Quantum Composers 9214 digital delay pulse generator (Quantum Composers, Bozeman, MT, USA) was used to synchronise the three cameras. Fast-start responses that were in the field of view of the three cameras were recorded with 470 frames per second. The used field of view resulted in a virtually unrestricted environment for the fish to move in, as the closest wall was at least $2L_{sl}$ away. Cameras were calibrated with direct linear transformation (DLT, method by Hedrick, 2008) by indicating the position of 72 points on a custom-designed 3D-printed frame (printed by Shapeways BV, Eindhoven, The Netherlands) for all cameras.

To elicit an escape response, a 103 g weight was dropped from the top of the aquarium using a manual electric switch when the fish was in the field of view, preferably in a still, steady and straight position. The stimulus was located in a fixed corner of the aquarium, 1 cm from the walls. The swimming arena was lit uniformly from the top using a LED panel. Similar panels on the side switched on when the stimulus was dropped, with a delay of a few milliseconds.

After being introduced into the swimming arena, fish were allowed to acclimatise for 10 min in the shade and 5 min with the top light turned on. Between stimuli, the fish were allowed a rest period of at least 5 min. A maximum of five escape responses were recorded per individual per day.

Fish tracking
The motion and deformation of the fish was reconstructed in 3D from each video with a branch of the Fish Tracker as described in Voesenek et al. (2016), written in MATLAB 2013a (The MathWorks, Natick, MA, USA). In the tracker, an *in silico* representation of the fish and experimental set-up is used to find the best possible fit of a fish model to the recorded video frames. This model consists of a tessellated 3D surface of the fish, with a specified position, orientation and body curvature. The experimental set-up is virtually recreated by calibrating the cameras (Hedrick, 2008). An image of the model fish is then projected onto the virtual cameras, showing how the high-speed video frames would look for a given set of parameters (i.e. position, orientation, curvature). The overlap between the projected image and the actual high-speed video frame gives an indication of the goodness-of-fit for this set of parameters. For every time instant in
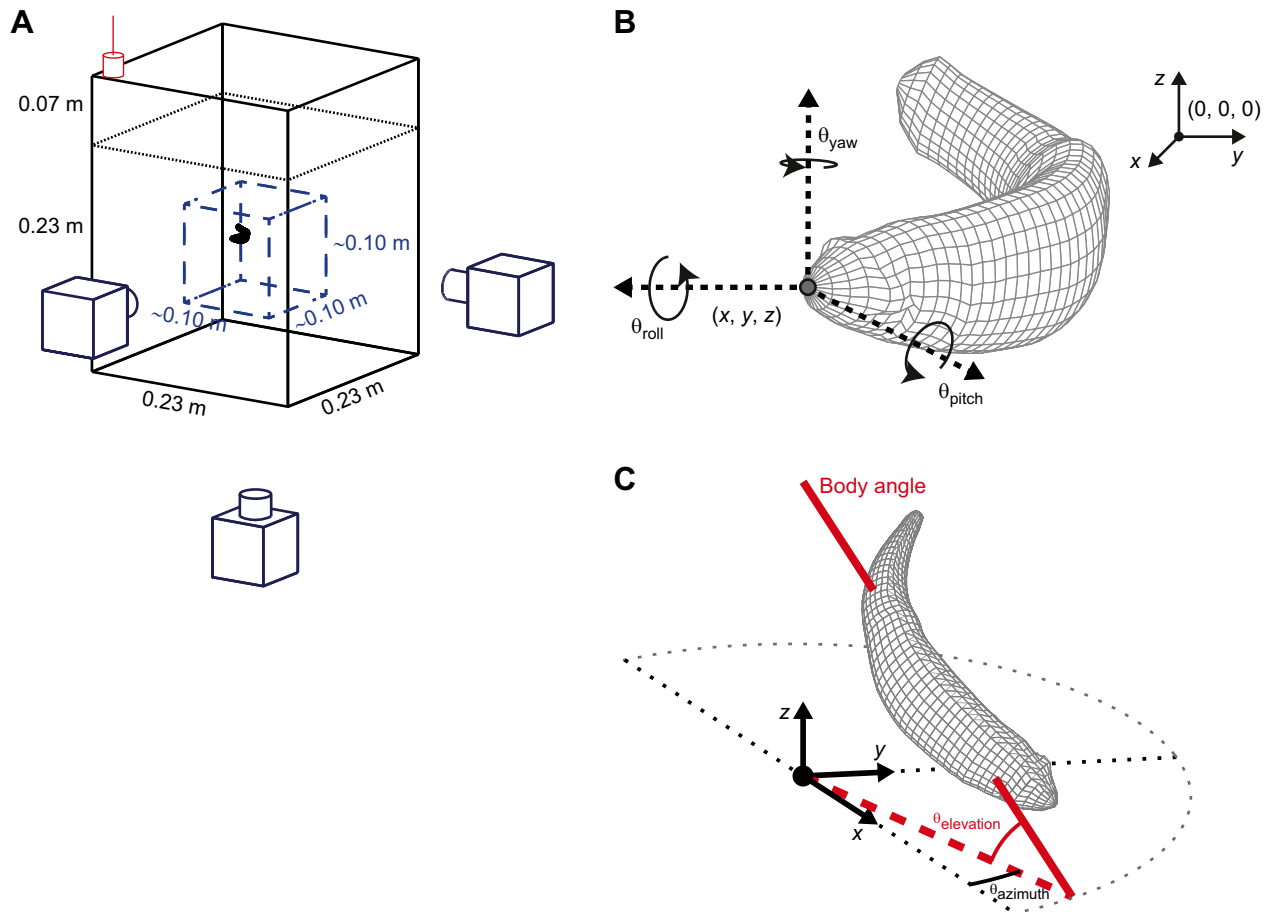
Fig. 1. Overview of the measurement set-up, three-dimensional angles and orientations. (A) The swimming arena allowed free swimming in all directions. The field of view (blue dashes) was located in the centre of the arena, and was recorded with three orthogonal cameras. The stimulus was given by dropping a weight at a fixed location in the corner of the tank. (B) Definition of the Tait–Bryan angles (θ: pitch, yaw and roll) of the head. (C) Azimuth and elevation angles ($\theta_{azimuth}$ and $\theta_{elevation}$) of the body angle.

the video sequence, the tracker uses an optimisation algorithm to find the combination of model parameters that result in this maximal overlap. Under the assumption of a uniform tissue density (1000 kg m^{-3}), the COM position and moment of inertia are calculated (Voesenek et al., 2016). This results in a time series of COM positions, body orientations and curvatures along the body. The reconstructed kinematics were smoothed with Whittaker smoothing ($\lambda=4$, order=0; Eilers, 2003). The result is a smooth series of 3D surfaces of the body at every point in time.

The 3D surface model of the fish was created from ventral and lateral pictures taken with two digital cameras (Nikon D3200, Tokyo, Japan; sensor resolution 24 Mpix) with macro lenses (Nikon Micro-NIKKOR 55 mm F/2.8, Tokyo, Japan; set to F/11), synchronized with a remote trigger (Jin Jia Cheng Photography Equipment, Shenzhen, China). In these images, outlines of the body, eye and abdomen were manually indicated in custom software written in MATLAB 2013a. These outlines were used to create ellipse-like cross-sections at 51 points along the body, similar to Voesenek et al. (2016). By connecting the series of cross-sections, a 3D surface model is formed. In this way, individual- and day-specific models were created of the fish, excluding the fins.

We prescribe the curvature at the posterior end of the body to be 0, as in the engineering case of a boundary condition for the free end of a bending beam. However, because we exclude the caudal fin, the posterior end of the model (i.e. the end of the caudal peduncle) is not

strictly equivalent to a free end. Hence, we greyed out the posterior 5% of all curvature plots, to indicate possible inaccuracies in this region.

A total of 437 escape response sequences were recorded. Following tracking and initial analysis, six movies were discarded due to inadequate tracking (bad model fit). We omitted 25 movies because the fish was moving while the response was elicited, 54 movies were excluded because no onset of motion was detected, and 29 movies were removed from further analysis as the fish did not exhibit a Stage 1 bend according to our objective criteria (see below for the criteria of stage transitions).

Head and body angles, and orientation changes

The head orientation was defined as the Tait–Bryan angles pitch, yaw and roll (Fig. 1B), calculated from the angle between the first two centreline segments of the head [see Voesenek et al. (2016) for a more detailed description]. Yaw angles were recalculated from the tracked rotation matrix, to prevent artefacts when these angles surpass 90 deg. The body angle in the yaw plane was derived from the yaw angle of each individual model segment, weighted by the contribution of each segment to the moment of inertia, and subsequently converted to world coordinates comparable to the head angle using the rotation matrix. Orientation of the fish was expressed in azimuth and elevation of the body angle axis (Fig. 1C).

Onset of motion and stage transitions

The transition between the different stages of the fast start was determined from the moment of inertia in the yaw plane (I_{yaw}), as this reflects whole-body curvature. Intermediate values of I_{yaw} were approximated by cubic spline interpolation, allowing sub-frame rate estimation of the transition point of each stage. The transitions between subsequent stages of the fast start (Stage 1→Stage 2, and Stage 2→Stage 3, respectively) were determined by locating the minima of I_{yaw} in MATLAB 2013a using the *findpeaks* function from the MATLAB Signal Processing Toolbox version 2013a ($-I_{yaw}$ for the negative peaks). We used a threshold on the magnitude of the moment of inertia to detect stage transitions. The following thresholds were used: transition from Stage 1→Stage 2: $0.97 \times$ maximum I_{yaw}; first peak of Stage 2 (fish moving back to a straight position): $1.1 \times I_{yaw,Stage1}$; transition from Stage 2→Stage 3: $0.99 \times I_{yaw,first peak Stage2}$. Stage 1 should follow within 30 frames ($\sim$64 ms) from the onset, while the two peaks of Stage 2 should follow within 15 frames ($\sim$32 ms) of the previous peak. As I_{yaw} is nearly insensitive to the initial head motion, we determined the beginning of Stage 1 of the fast-start manoeuvre from the change in yaw angle of the head, i.e. the last change of sign of the derivative of the yaw angle preceding the end of Stage 1. A total (N_D) of 133 movies fitted to all the above criteria.

Single-bend and double-bend starts

The recorded fast-start sequences could be divided into three groups: starts in which the fish did not exhibit the contralateral tail-beat characteristic of Stage 2 [single-bend (SB) fast starts], events in which the fish did [double-bend (DB) fast starts, e.g. Figs 2 and 3], and residual manoeuvres that did not fit all the criteria for the aforementioned categories. Starts from the former two groups were analysed separately (results of SB in Figs S1 and S2). To define the 'end' of SB starts, we used the time point where the time derivative of I_{yaw}, following a negative and positive peak, returned within a narrow range around the initial values (Fig. S2A), which should occur within 30 frames ($\sim$64 ms) after the onset of motion. This range spans from two times the minimum of the derivative of I_{yaw} to two times its maximum in the five video frames ($\sim$11 ms) preceding the onset of motion. This criterion is roughly comparable to the 'first peak' during Stage 2 of DB starts;
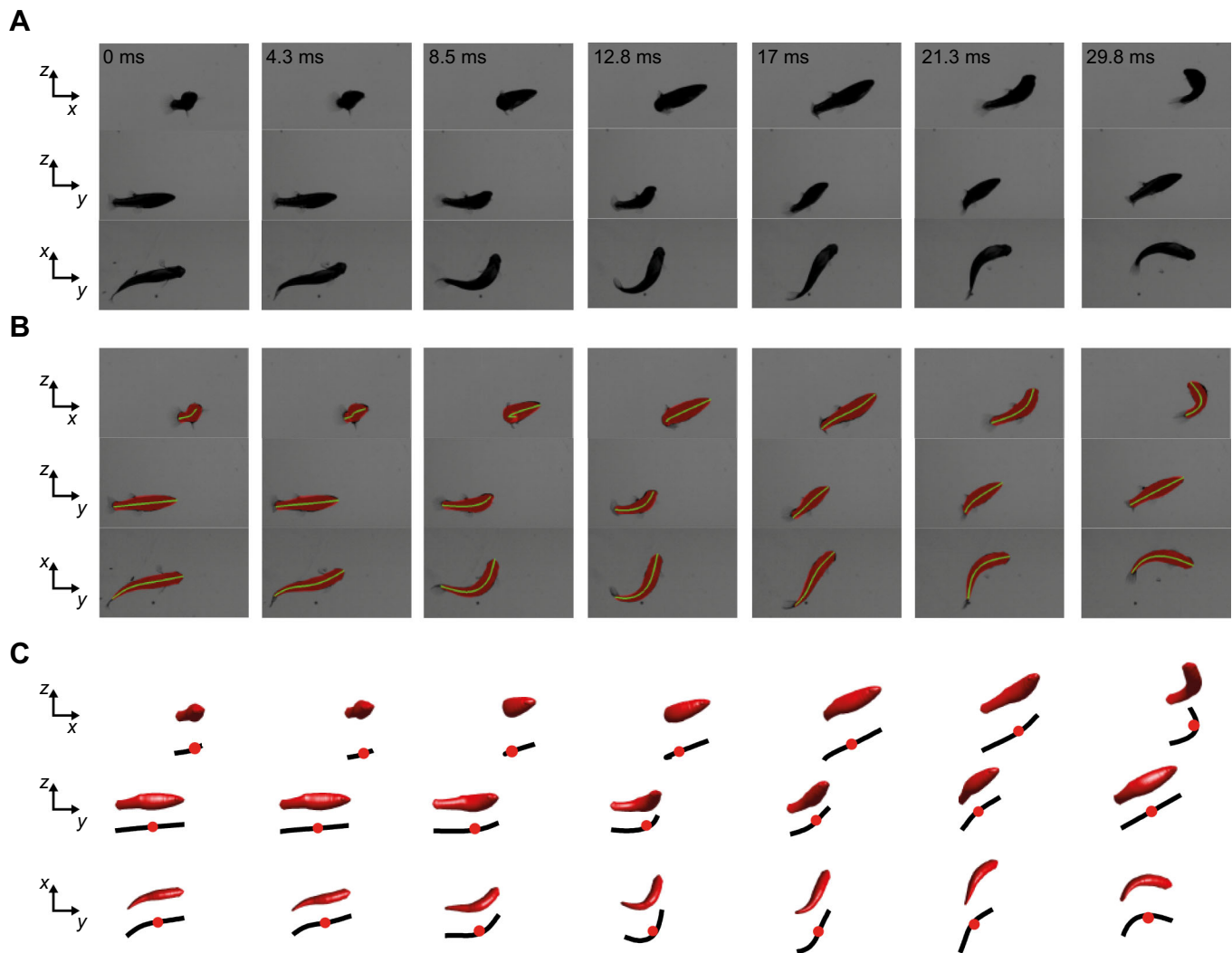
Fig. 2. Overview of a typical three-dimensional double-bend fast-start manoeuvre with an upwards pitch in *Heterandria formosa*. (A) Raw movie images from the three orthogonally oriented cameras. The top two rows show horizontal views, the third row displays images from the bottom view. Images are cropped to show only the region of motion. (B) The same frames with an overlay of the fitted body model (red) and centre line (green) for the respective cameras. (C) 3D body representations for the above image frames; centre lines (black) and position of the centre of mass (red dot) are displaced vertically for visibility.
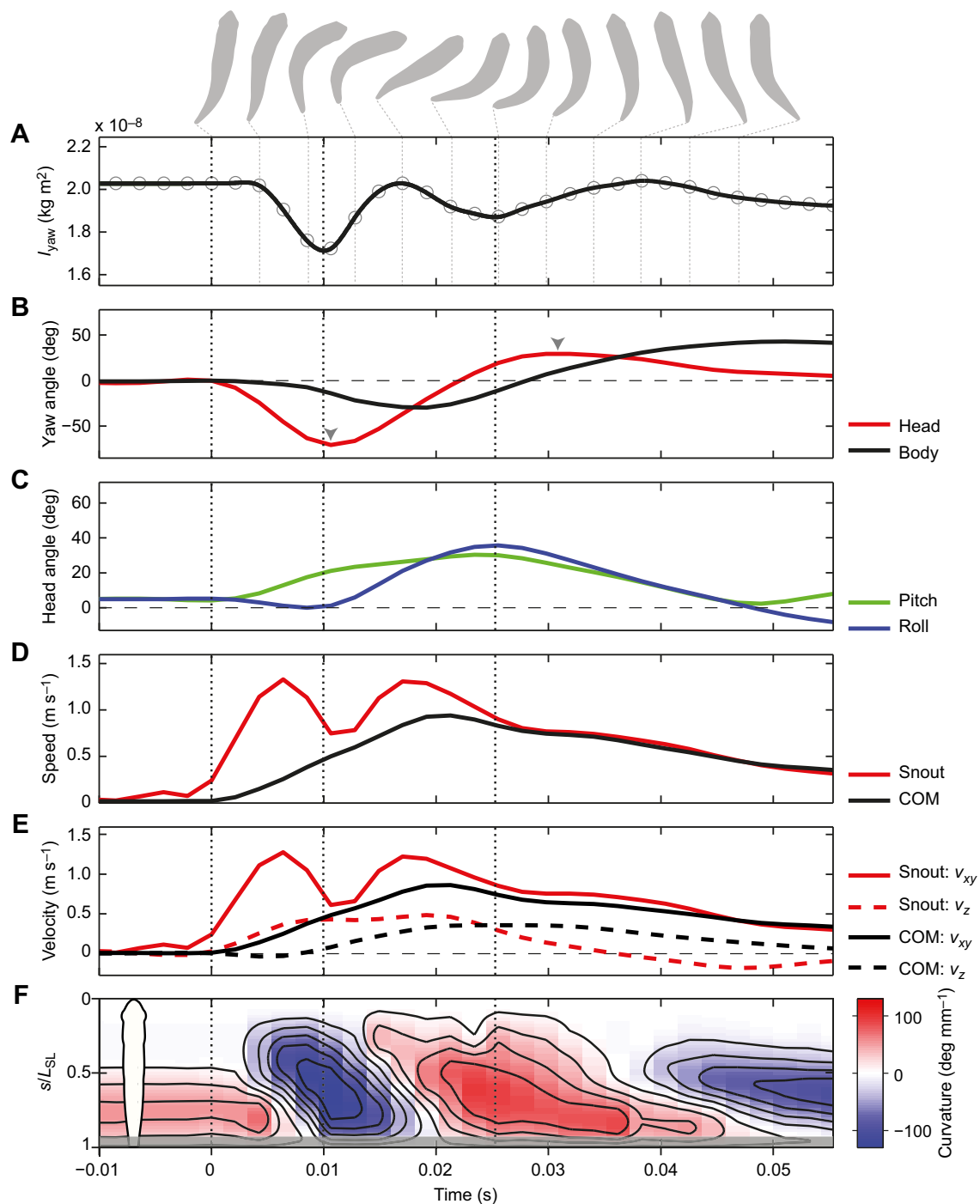
Fig. 3. Kinematic variables from the double-bend fast-start manoeuvre displayed in Fig. 2. Onset of motion, the transition from Stage 1→Stage 2, and the transition from Stage 2→Stage 3 are depicted by vertical black dotted lines (from left to right, respectively). Time is set to 0 s at the onset of motion. (A) Moment of inertia in the yaw plane (I_{yaw}) during the manoeuvre. The negative peaks in I_{yaw} are used to determine the end of Stage 1 (second black dotted line) and the end of Stage 2 (third black dotted line); hereafter the manoeuvre continues with a variable Stage 3, in this example a weak tail beat. The continuous black line represents a cubic spline fit of the data (represented by the open circles). A bottom view of the body of every second frame is depicted at the top of the figure; displacement of the body is not shown. (B) Change in yaw angle of the head and body over time. Grey arrowheads indicate local peaks in the yaw angle change of the head. These moments have been used in previous approaches as the ends of Stage 1 and Stage 2, respectively. (C) Change in pitch and roll angles of the head during the fast-start manoeuvre. (D) Absolute speed measured at the snout and at the centre of mass (COM). (E) Velocity (v) split up into horizontal and vertical components for the snout (red) and COM (black), respectively. (F) Curvature along the body over time. s/L_{SL} is the relative position along the body, with 0 being the head and 1 being the posterior end of the caudal peduncle. In B, C and E, horizontal dashed lines are a projection of y=0.

we named this kinematic time point 'SB$_{end}$'. A total (N_S) of 75 recorded manoeuvres fitted these criteria for a complete SB manoeuvre. The number of residual events (N_R) that were analysed

was 121; five of these events were not analysed because the fish moved out of the field of view within 32 ms after the onset of motion.

Mean effective acceleration

To determine whether Stage 1 contributes to a 'useful' propulsion, i.e. in the direction of the final escape, we calculated the mean effective acceleration of the COM during Stage 1 and Stage 2 of the fast start. The mean effective acceleration was calculated by taking the dot-product of the mean acceleration of each stage and the velocity unit vector of the COM at the end of Stage 2. We defined usefulness from a performance perspective: if there is a positive mean effective acceleration during a stage, it has a positive contribution to the escape velocity at the end of Stage 2. Other aspects of the fast start (e.g. unpredictability) might benefit from negative mean accelerations; this is outside of the scope of this study, however.

Statistics

Raw kinematic data and the derived data on head angles, orientation and heading have been submitted to the Dryad Digital Repository and can be found at http://dx.doi.org/10.5061/dryad.qb5j6 (Fleuren et al., 2018). Linear mixed models were used to determine relationships between angles and orientations using *proc mixed* for SAS 9.3 (SAS Institute, Cary, NC, USA). This statistical method accounts for repeated measures within individuals (Singer, 1998). Differences between effective acceleration of Stages 1 and 2 were determined using *proc univariate* for SAS 9.3. Correlations between orientation of the fish and heading were calculated with the *circular correlation* function from the *circular* macro (Kölliker and Richner, 2004) in SAS 9.3. The used non-parametric correlation coefficient (r_n) is analogous to Spearman's correlation coefficient (Fisher and Lee, 1982). All the above analyses were performed on events with both Stage 1 and Stage 2 (or SB_{end}) defined. Two-sample *t*-tests were performed with the *ttest2* function and Wilcoxon rank sum tests were performed with the *ranksum* function, both part of the Statistics and Machine Learning Toolbox 2013a for MATLAB 2013a. Differences were considered significant if $P<0.05$.

RESULTS

Example of a 3D fast start

The analysed DB fast-start manoeuvres of *H. formosa* are characterized by a 'C-bend' in Stage 1, followed by forward propulsion in Stage 2, and a variable third stage (example in Fig. 2): changes in 3D orientation can occur during all three stages. The end of Stage 1 and Stage 2 was determined from minima in the moment of inertia in the yaw plane (I_{yaw}) (Fig. 3A). The body angle is phase shifted with respect to the angle of the head, and has a smaller amplitude: overall body orientation is changing less rapidly than the orientation of the head (Fig. 3B). Changing pitch and roll angles of the head reflect the 3D nature of the fast-start manoeuvre (Fig. 3C). The pitch angle of the head increases during both Stages 1 and 2, while in this example the roll angle remains almost constant during Stage 1, but increases in Stage 2 to 35 deg (Fig. 3C).

The speed of the snout increases rapidly after the onset of motion (Fig. 3D), linked to the rotation and displacement of the head. The speed of the COM lags, but is already considerable at the end of Stage 1 in this example (Fig. 3D). The pattern of the speed curves differs between head and COM-based systems: the absolute speed of the snout shows two characteristic peaks in both Stage 1 and Stage 2 that reflect the lateral velocity (Fig. 3E), while the speed of the COM increases almost steadily and reaches its peak 4.5 ms before the end of Stage 2 (Fig. 3D). The speed drops after Stage 2; in other cases Stage 2 can be followed by further tail beats in Stage 3 and a concomitant rise in velocity. The vertical velocity of the snout increases during Stage 1 and levels off during Stage 2 during this particular manoeuvre (Fig. 3E). The COM displaces very little in the

vertical direction during Stage 1, but vertical velocity increases steadily during Stage 2 (Fig. 3E). The body curves heavily in different directions during Stage 1 and Stage 2, with curvature travelling along the body as a wave (Fig. 3F), similar to previous observations (e.g. Wakeling and Johnston, 1998; Müller and Van Leeuwen, 2004; Nair et al., 2015).
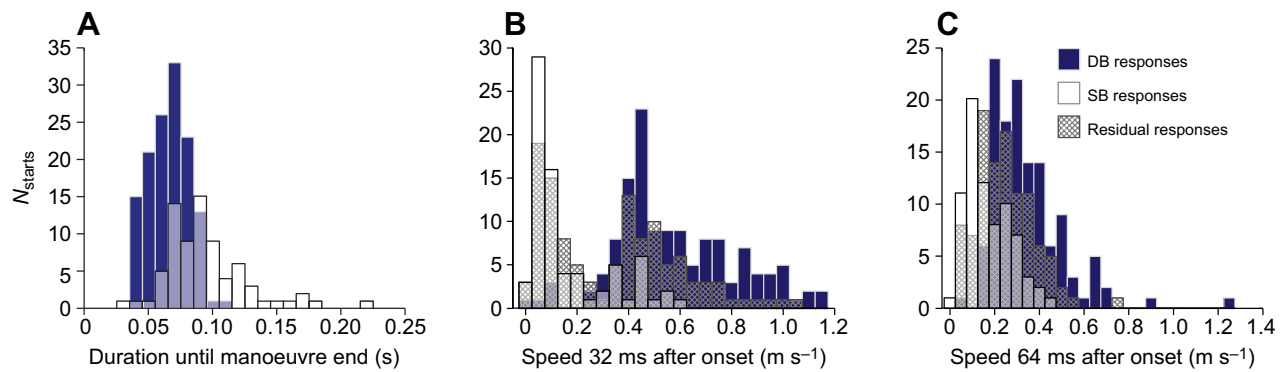
Single-bend and double-bend fast starts

In 196 out of 329 analysed manoeuvres, we did not detect a second minimum in I_{yaw}, indicating a lack of the contralateral bend (Fig. 4A). In these starts, the fish slowly straightens its tail after the initial C-bend. This difference in kinematics is also reflected in the plots of body curvature (Fig. 4B), where the SB start is characterized by one large curvature wave, whereas the DB start shows two travelling curvature waves along the body during the first two stages of the fast start. In general, the attained speed of the COM is higher in DB responses than in SB responses, as is the attained change in yaw angle in this period (Fig. S1A–D). The two types of starts do not differ significantly in their average change in pitch and roll angle, but the attained pitch angle during Stage 1 is lower in SB responses than in the residual responses (Fig. S1E,F). The results of SB starts that fulfilled our criteria for an objective end-point (SB_{end}, see Materials and Methods) are given in the supplementary information (Fig. S2, Table S1).

SB responses tend to take longer to complete than DB responses (Fig. 5A) and the COM often has a lower speed when measured at fixed time points, e.g. at 32 and 64 ms after onset (Fig. 5B and C, respectively). The speed of fish exhibiting a residual response (without detected objective end-points) forms a bimodal distribution at 32 ms (Fig. 5B), which occupies almost the same range as the sum of the distributions of the SB and DB starts. The 'residual' distribution is intermediate between SB and DB responses at 64 ms after the onset of motion (Fig. 5C). Overall, the mean performance of fish exhibiting a residual response is intermediate between SB and DB responses (Fig. S1).
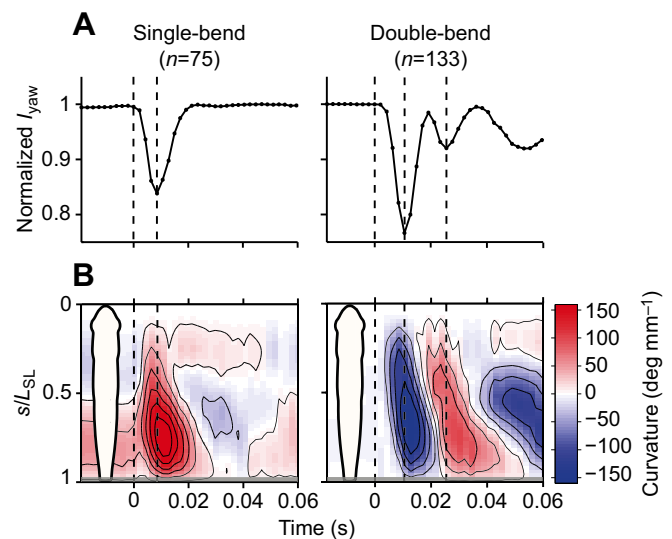
Fig. 4. Example of the differences between single-bend and double-bend fast starts. (A) Plots of the in-plane moment of inertia (I_{yaw}) over time, normalized by maximum I_{yaw} for comparison, for an example of a single-bend fast start (left) and a double-bend fast start (right). (B) Curvature plots of the sequences in A. Dashed vertical lines represent the beginning and end of the stages of the fast start (onset at t=0 ms). s/L_{SL} is the relative position along the body, with 0 being the head and 1 being the posterior end of the caudal peduncle.

Fig. 5. Duration of fast-start manoeuvres and fast-start performance at a fixed point in time. N_D=133 manoeuvres, N_S=75 manoeuvres, N_R=116 manoeuvres; from 14 individuals. (A) Duration of identified double-bend (DB) and single-bend (SB) responses until the respective kinematic end-points (see Materials and methods) are reached. (B) Speed of the centre of mass 32 ms after the onset of motion for the SB, DB and residual starts. (C) Speed of the centre of mass 64 ms after the onset of motion.

Variation in fast-start kinematics

During the first two stages of the DB fast start, the snout and the COM exhibit different patterns in angles and speeds. The snout undergoes large displacements during both Stage 1 and Stage 2, while the displacement of the COM is much larger in Stage 2 than in Stage 1 (Fig. 6A). These differences are reflected in the horizontal speed during the different stages: the horizontal speed of the snout is mostly larger in Stage 1 than in Stage 2, as indicated by their position below the isoline, while the COM attains higher velocities during Stage 2 (Fig. 6B). A similar pattern is visible for the vertical velocity: the snout attains larger vertical velocities than the COM during Stage 1 (Fig. 6C), but overall the magnitude is lower than for horizontal speed. SB starts show comparable trends when comparing from the onset of motion until the end of Stage 1, and
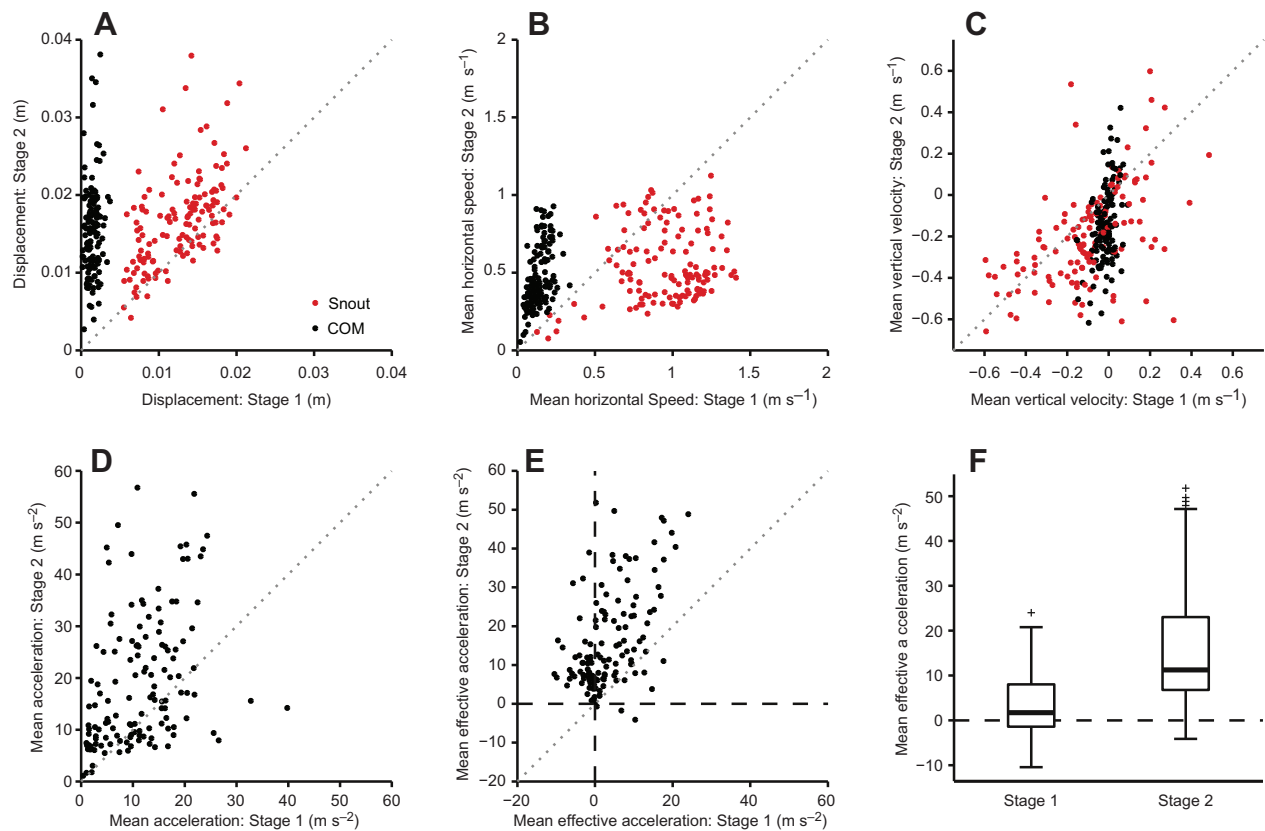
Fig. 6. Displacement, mean speed, mean velocity and mean acceleration during Stage 1 and Stage 2 of the double-bend fast starts. N_D=133 responses, from 14 fish. (A) Displacement of the snout (red) and centre of mass (COM; black) during Stage 1 and Stage 2 of the fast start. (B) Mean horizontal speed of the snout (red) and COM (black) during Stage 1 and Stage 2 of the fast start. (C) Mean vertical velocity of the snout (red) and COM (black) during Stage 1 and Stage 2 of the fast-start. (D) Mean acceleration of the COM during Stage 1 and Stage 2 of the fast start. (E) Mean effective acceleration of the COM during Stage 1 and Stage 2 of the fast start. (F) Box plot of the mean effective acceleration of the COM during Stage 1 and Stage 2 of the fast start. Bottom and top edges of the box indicate the 25th and 75th percentile of the data, respectively; middle line indicates the median; whiskers indicate ∼99% of the data. Crosses mark individual outlier data points. (A–E) Dotted line represents $x=y$ isoline.

from the end of Stage 1 until SB$_{end}$ (Fig. S2B–D), albeit the maximum attained values are lower.

At a fixed point in time from the onset of motion (32 ms from the onset of motion), it is clear that there is large variation between the manoeuvres, both in displacement of the COM and in speed of the COM (Fig. S3A–C). On average, the SB starts are slower and undergo a smaller displacement within a given time frame than DB fast starts and the residual responses.

The COM accelerates during both Stage 1 and Stage 2 in DB manoeuvres (Fig. 6D), and during both Stage 1 and the period between the end of Stage 1 and SB$_{end}$ in SB starts (Fig. S2E). However, this acceleration is not always in the direction of the final escape, as determined from the velocity vector of the COM at the end of Stage 2: in a substantial fraction of the manoeuvres (50 out of 133 DB responses), the COM had a negative mean effective acceleration during Stage 1 (Fig. 6E). During Stage 2, the COM generally has a positive mean effective acceleration. On average, the mean effective acceleration of the COM is larger than 0 during both Stage 1 (mean±s.e.m.: 3.47±0.61 m s^{-2}, t-test: $P<0.001$, $N=133$) and Stage 2 (15.86±1.10 m s^{-2}, t-test: $P<0.001$, $N=133$), but Stage 2 has a larger mean effective acceleration than Stage 1 (difference of means: 12.39 m s^{-2}; Wilcoxon signed rank test: $P<0.001$, $N=133$).

In DB starts, the snout moves laterally in Stage 1, followed by a contralateral motion in Stage 2. This is reflected by the observed pattern in yaw angle of the head: the yaw angle of Stage 2 generally has the inverse sign of the yaw angle of Stage 1 (Table 1, Fig. 7A; range of yaw angle change: Stage 1, −178 to 169 deg; Stage 2, −110 to 115 deg). The yaw angle of the body, however, has the same sign at the end of Stage 1 and Stage 2, as the orientation of the body changes more slowly and eventually converges with the head angle at the end of Stage 2 (see for example Fig. 2B). There is a negative correlation between the change in pitch angle in Stage 1 and Stage 2

(range of pitch angle change: Stage 1, −43 to 37 deg; Stage 2, −25 to 43 deg), but the change in roll angle of the head during the two stages of the fast start are uncorrelated (Table 1, Fig. 7B,C; range of roll angle change: Stage 1, −52 to 45 deg; Stage 2, −78 to 58 deg).

In SB starts, the head barely moves in the yaw direction between the end of Stage 1 and SB$_{end}$ (Fig. S2F). Head movements in the yaw plane are significantly correlated during these two stages (Table S1). In contrast to DB starts, the relationship between the change of yaw angle during Stage 1 and between the end of Stage 1 and SB$_{end}$ is positive in SB manoeuvres: the head keeps moving in the same (yaw) direction during both stages. Changes in pitch and roll angles of the head are not correlated between the two compared stages of SB manoeuvres (Fig. S2G,H; Table S1). During the first 32 ms of the fast-start manoeuvre, there are large variations in all three head angle directions for both SB and DB manoeuvres, as well as for the residual manoeuvres (Fig. S3D–F).

Changes in 3D orientation and heading

Yaw, pitch and roll of the head during the different stages of the DB fast start correlate differently with the attained escape directions. The azimuth change during the fast-start manoeuvre correlates positively with the change in yaw angle of the head during Stage 1 and the change in yaw angle of Stages 1 and 2 combined, but negatively with the change in yaw angle during Stage 2 alone (Table 1, Fig. 8A). During Stage 2, the head moves in the opposite (yaw) direction from Stage 1 (Fig. 7A). Elevation change is positively correlated with changes in pitch angle of the head during Stage 2 and during Stage 1 plus Stage 2 (Table 1, Fig. 8D). Neither azimuth nor elevation change correlate with changes of the roll angle of the head (Table 1, Fig. 8B,C). The range of attained roll angles is relatively small during each of the stages of the fast-start manoeuvre: with the exception of a few outliers, the roll change

Table 1. Mixed model outputs for correlations between Tait–Bryan angles pitch, yaw and roll of the head and position changes of the centre of mass in the world coordinate system (azimuth and elevation)

	Model		Intercept			Slope		
	F	P-value	Estimate	s.e.	P-value	Estimate	s.e.	P-value
Pitch, yaw and roll angles: correlation between Stage 1 and Stage 2								
Yaw$_{head}$ (1–2)=int+slp Yaw$_{head}$ (O–1)	$F_{1,129}$: 31.93	<0.0001	−7.34	3.88	0.0814	−0.19	0.03	<0.0001
Pitch$_{head}$ (1–2)=int+slp Pitch$_{head}$ (O–1)	$F_{1,128}$: 4.79	0.0305	8.79	1.65	<0.0001	−0.20	0.09	0.0305
Roll$_{head}$ (1–2)=int+slp Roll$_{head}$ (O–1)	$F_{1,130}$: 2.90	0.0909						
Yaw$_{body}$ (1–2)=int+slp Yaw$_{body}$ (O–1)	$F_{1,130}$: 493.59	<0.0001	−4.07	2.18	0.0640	1.12	0.05	<0.0001
Correlation between changes in pitch, yaw and roll angles and position changes in the world coordinate system								
Azi (1–2)=int+slp Yaw (O–1)	$F_{1,130}$: 1745.36	<0.0001	−1.22	2.24	0.5853	0.94	0.02	<0.0001
Azi (1–2)=int+slp Yaw (1–2)	$F_{1,130}$: 15.32	0.0001	2.70	8.16	0.7416	−0.73	0.19	0.0001
Azi (1–2)=int+slp Yaw (O–2)	$F_{1,129}$: 703.76	<0.0001	7.40	3.63	0.0727	1.00	0.04	<0.0001
Azi (1–2)=int+slp Roll (O–1)	$F_{1,130}$: 2.81	0.0958						
Azi (1–2)=int+slp Roll (1–2)	$F_{1,130}$: 0.19	0.6640						
Azi (1–2)=int+slp Roll (O–2)	$F_{1,130}$: 2.18	0.1426						
Azi (1–2)=int+slp Pitch (O–1)	$F_{1,130}$: 1.61	0.2066						
Azi (1–2)=int+slp Pitch (1–2)	$F_{1,130}$: 0.00	0.9447						
Azi (1–2)=int+slp Pitch (O–2)	$F_{1,130}$: 1.02	0.3142						
Elev (1–2)=int+slp Yaw (O–1)	$F_{1,129}$: 2.51	0.1158						
Elev (1–2)=int+slp Yaw (1–2)	$F_{1,130}$: 0.22	0.6384						
Elev (1–2)=int+slp Yaw (O–2)	$F_{1,129}$: 2.35	0.1275						
Elev (1–2)=int+slp Roll (O–1)	$F_{1,129}$: 0.14	0.7086						
Elev (1–2)=int+slp Roll (1–2)	$F_{1,128}$: 1.09	0.2994						
Elev (1–2)=int+slp Roll (O–2)	$F_{1,130}$: 0.43	0.5137						
Elev (1–2)=int+slp Pitch (O–1)	$F_{1,130}$: 2.89	0.0918						
Elev (1–2)=int+slp Pitch (1–2)	$F_{1,129}$: 27.00	<0.0001	0.35	2.32	0.8825	0.68	0.13	<0.0001
Elev (1–2)=int+slp Pitch (O–2)	$F_{1,120}$: 32.10	<0.0001	−1.05	2.19	0.6369	0.59	0.10	<0.0001

All relationships except azimuth–pitch and elevation–yaw are plotted in Figs 7 and 8. Model: type 3 test of fixed effects. Azi, azimuth; Elev, elevation; int, intercept; slp, slope; s.e., standard error of the estimate. Change between time points indicated in parentheses: O, onset of motion; 1, end of Stage 1; 2, end of Stage 2.
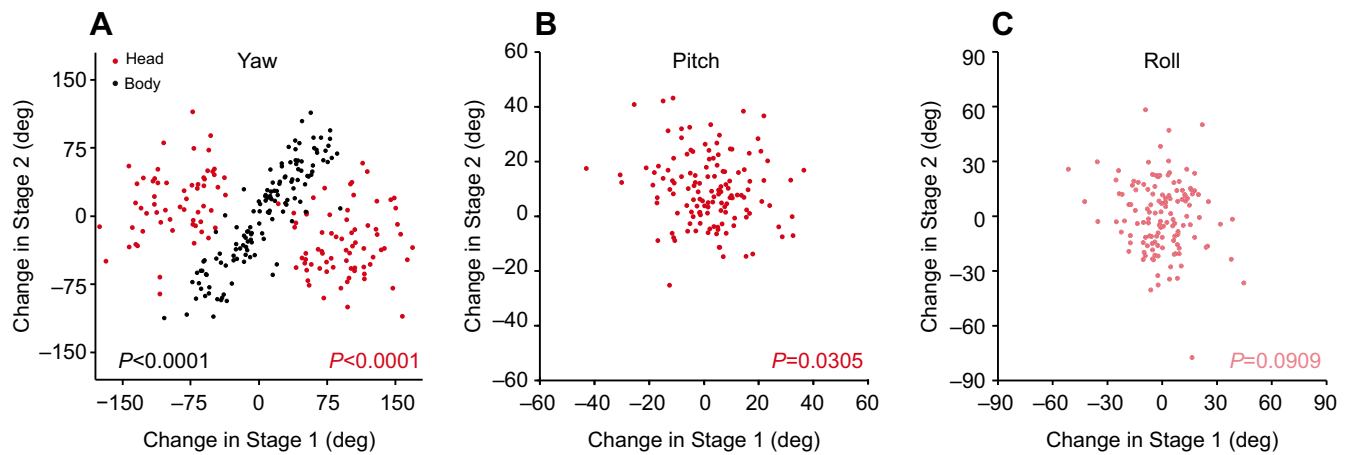
Fig. 7. Tait–Bryan angle changes during the two stages of the double-bend fast starts. N_D=133 responses, from 14 fish. (A) Yaw angle changes of the head (red) and body (black) show different correlations between Stage 1 and Stage 2. (B) Pitch angle change of the head during Stage 1 and Stage 2. (C) Roll angle change of the head during the two stages of the fast-start manoeuvre.

during any of the stages is often limited to ±30 deg (Fig. 8B,C). Without large changes in roll, yaw angle changes of the head are connected to angular changes of the body in the horizontal plane of the world coordinate system and pitch angle changes are strongly reflected in the vertical plane. As a result, the yaw angle change of the head correlates with azimuth change of the body and, similarly, pitch angle change with elevation change. Furthermore, yaw angles of the head do not correlate with the attained elevation change of the body during the fast start, nor do pitch angles correlate with the attained azimuth change (Table 1).

Escape heading is described in azimuth and elevation coordinates determined from the velocity vector at the end of Stage 2 of DB starts (Fig. 9A). Initial orientation of the fish with respect to the stimulus does not limit the range of azimuth directions the fish escapes in (Fig. 9B; non-parametric circular correlation coefficient r_n=0.00378, P=0.600, 5000 permutations). There is an effect of initial elevation with respect to the stimulus and elevation of final heading, indicating that fish that have a negative initial elevation towards the stimulus are more likely to aim their escape directions (further) downwards (Fig. 9C; r_n=0.06121, P≤0.001, 5000 permutations).

In SB manoeuvres, the correlations between initial orientation and final heading are different: the azimuth of the heading is significantly (positively) correlated with initial orientation (Fig. S2I; non-parametric circular correlation coefficient r_n=0.24979, P<0.001, 5000 permutations), while for elevation they are not (Fig. S2J; r_n=0.02795, P=0.124, 5000 permutations).

DISCUSSION
Adult *H. formosa* vary the direction of their fast-start escape manoeuvre in three dimensions, adding variety to their achieved escape directions. The literature on the 3D nature of fast-start responses in adult fish is sparse (Eaton et al., 1977: one sequence; Kasapi et al., 1993: 14 sequences), and the data presented here expand our knowledge on the range of possible escape headings. The maximum attained pitch and roll angles reported by Kasapi et al. (1993) for fast starts of knifefish fall in the range of pitch values reported here. Our results build upon the results of Nair et al. (2015), who show that the fast-start manoeuvres of larval zebrafish can be 3D in nature. Here, we have quantitatively shown that there is also a large variation in the 3D re-orientation during the fast-start responses of adult fish.

Variation in 3D escape orientation and heading
We provided a stimulus from a fixed position in the swimming arena, always exciting the fish from above. The fish responded with a variety of escape angles, with azimuth angle changes of the body spanning from −219 to 172 deg and elevation changes of the body ranging from −51 to 63 deg in DB starts (Fig. 8). For the changes in azimuth, this is probably due to natural variation in escape angle: the escape heading is unrelated to the initial orientation of the fish with respect to the stimulus in DB manoeuvres (Fig. 9B), but not in SB manoeuvres (Fig. S2I). The elevation of the heading of the fish at the end of Stage 2 is correlated with elevation of the fish at the onset in DB manoeuvres (Fig. 9C): with the stimulus coming from the top, the fish are likely to escape (further) down. In SB fast starts, the elevation of the heading is not correlated with the orientation at the onset of motion (Fig. S2J). This is an important distinction between SB and DB manoeuvres and could merit further research: our data indicate that SB responses are less variable in the horizontal plane (azimuth), but are more variable in the vertical plane (elevation).

Our results for DB manoeuvres match findings in larval zebrafish: they respond with a downwards oriented escape direction when positioned to the ventral side of an approaching predator (Stewart et al., 2013). Larvae that were positioned at the dorsal side respond with an escape in the horizontal plane; whether such a distinction holds for adult fish is still unconfirmed. Our dataset contains multiple upwards directed fast-start responses, indicating that there is no kinematic restriction for upwards directed escape responses.

In natural situations, predators may approach a prey from any orientation in 3D space: some predators preferentially strike from above (e.g. birds), others attack mostly from below (e.g. bottom-dwelling fish), and others prefer to strike in a (nearly) horizontal plane. How prey fish respond to different strike orientations in 3D space is to our knowledge still unknown, despite its ecological relevance. Previous studies on the kinematics of fast-start responses in adult fish have largely neglected vertical escape directions, as the fast start was considered a planar motion (Domenici and Blake, 1997). This was reflected in experimental designs, with the responses studied in shallow water in which vertical motion was restricted, and/ or with video recordings from a dorsoventral perspective that do not allow quantification of changes in elevation. Only two previous studies have reported fast-start manoeuvres out of the horizontal plane in adult fish, in the hatchetfish (Eaton et al., 1977) and in the knifefish
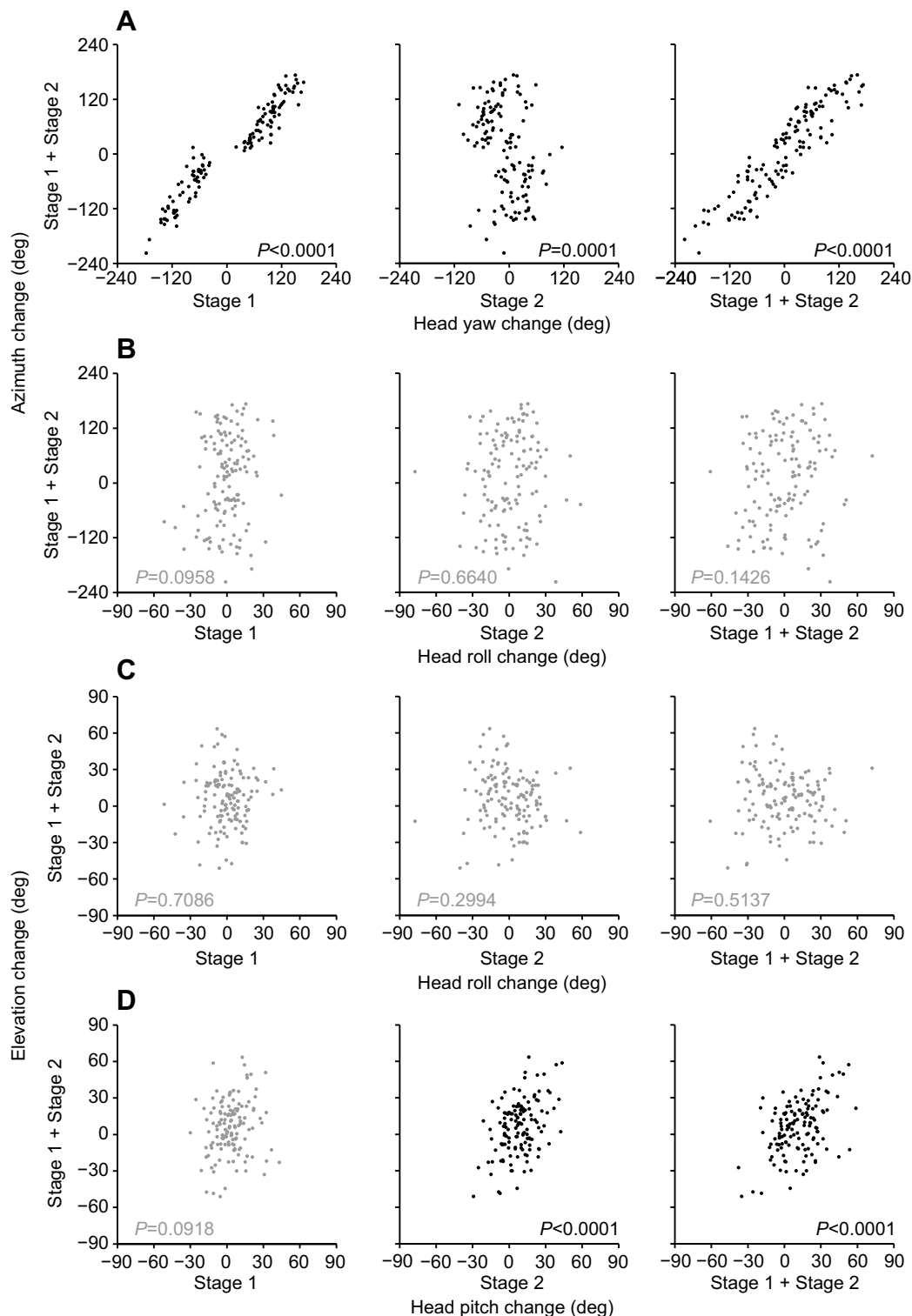
Fig. 8. Relationship between head angle change during the different stages of the double-bend fast starts and change in orientation of the body between the onset of motion and the end of Stage 2. N_D=133 responses, from 14 fish. Mixed model estimates for the correlations are given in Table 1; significant correlations are plotted in black, insignificant correlations are plotted in grey; corresponding *P*-values are displayed in the bottom right- and left-hand corners, respectively. (A) Change in azimuth of the body is correlated with changes in yaw angle of the head during Stage 1, Stage 2 and Stage 1+2. (B) Change in azimuth is not correlated with changes in roll angle of the head. (C) Changes in elevation are not correlated with changes in roll of the head. (D) Change in elevation of the body during the fast start is positively correlated with changes in pitch angle of the head during Stage 2 and Stage 1+2, but not with Stage 1.

(Kasapi et al., 1993). Both these fish species have a substantially different morphology compared with most other fish species; our data show that fish with a typical body shape can also exhibit fast starts

with a large 3D component. Our data furthermore show considerable variation in 3D escape headings that could affect the outcome of predator–prey interactions (Domenici et al., 2011a,b).
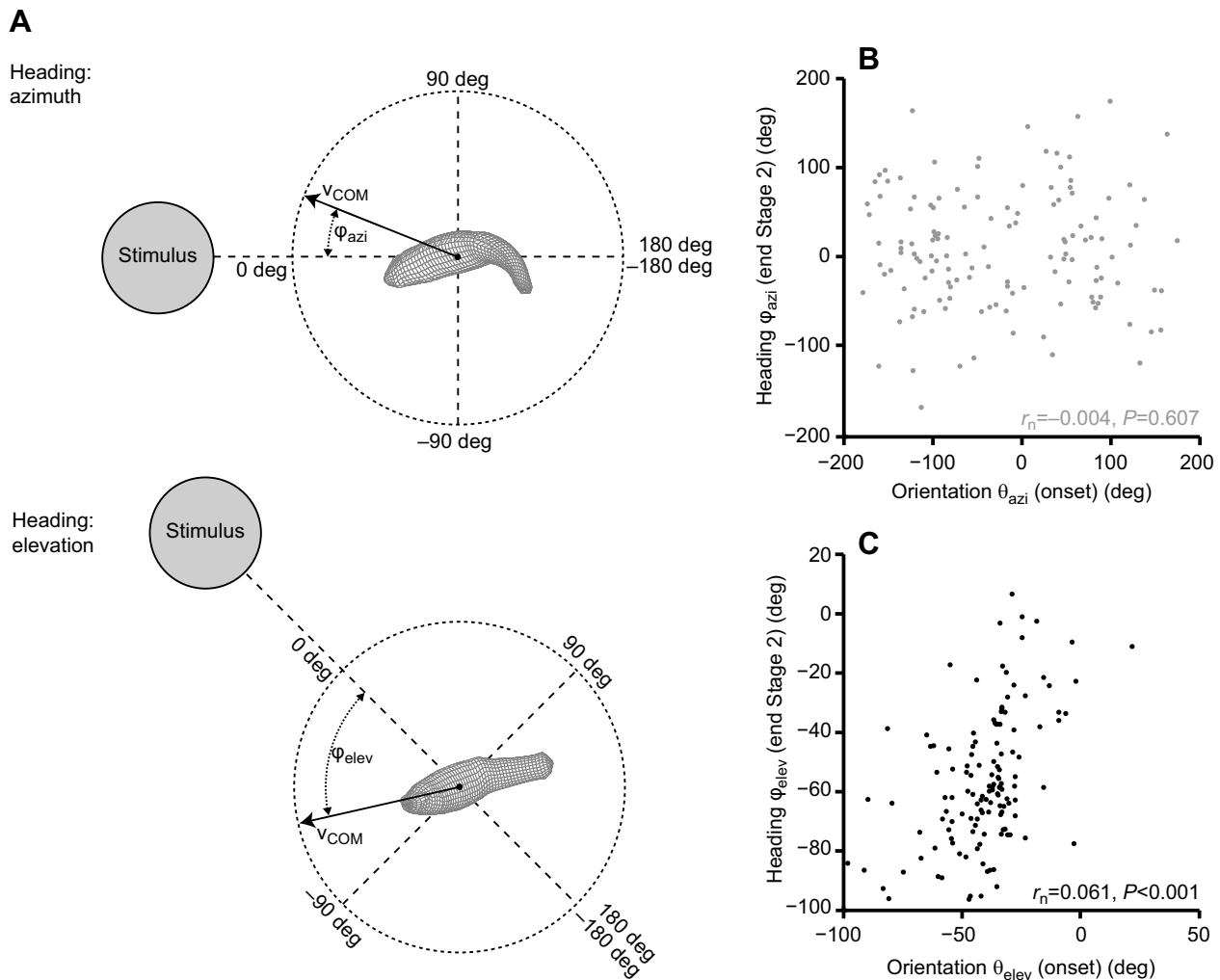
Fig. 9. Correlation between initial orientation of the fish with respect to the stimulus, and escape heading at the end of Stage 2 of the double-bend fast starts. N_D=133 responses, from 14 fish. Significant correlations are plotted in black, insignificant correlations are plotted in grey; correlation coefficient r_n and P-values are displayed in the bottom right-hand corners. (A) Explanation of escape heading: azimuth and elevation are 0 deg when the velocity vector of the centre of mass (COM) faces the stimulus, and (−)180 deg when it faces directly opposite. (B) The azimuth heading at the end of the fast start is not correlated with the orientation of the fish at the onset of motion. (C) The elevation heading at the end of the fast start is positively correlated with the orientation of the fish at the onset of motion.

Using the moment of inertia to determine the kinematic end-points of fast-start manoeuvres

During a fast-start manoeuvre, the whole fish bends in 3D space (see, for instance, the example in Figs 2 and 3). For this reason, it makes sense to take into account the whole body when describing the different kinematic stages. We opted to do this by determining the transition from Stage 1 to Stage 2, from Stage 2 to Stage 3 (for DB fast starts), and the kinematic end-point of SB starts with the moment of inertia in the yaw plane (I_{yaw}). The extrema in I_{yaw} correspond to peaks in whole-body curvature (Figs 3 and 4). This novel approach leads to slightly different timings for the ends of the different stages of the fast-start manoeuvre than obtained with previous methods [e.g. the change in turning angle of the head used by Kasapi et al. (1993); Spierts and Van Leeuwen (1999); and Goldbogen et al. (2005) among others; see arrowheads Fig. 3B]. In the example of Fig. 3, the difference between the two methods is most pronounced at the end of Stage 2, which is shorter with the I_{yaw} approach. Using I_{yaw} to determine the stage end-points comes with two downsides. Firstly, I_{yaw} is relatively insensitive to small motions in the head and/or tail. As a result, detecting the onset of motion

using whole-body moment of inertia is outside the possibilities of the spatial and time resolution used in this study. However, as the head region is usually one of the first to rotate during a fast start (e.g. Müller and Van Leeuwen, 2004; Li et al., 2014), changes in head angle can be used to detect the onset of motion (see Materials and Methods). Secondly, not all starts could be assigned to one of the two fast-start categories: single-bend and double-bend manoeuvres. This could be the case when a fish does not completely stretch straight following Stage 1, i.e. it glides or brakes with a curved body. Under these conditions, our criteria for objective end-points are not met.

Does Stage 1 add to propulsion?

Stage 1 of the fast-start manoeuvre plays an important role in the re-orientation of the body, both in azimuth and elevation directions (DB starts; Fig. 8) and provides initial conditions of body curvature and tail fin orientation for Stage 2 that favour propulsion in the subsequent tail beat. For this reason, this stage has often been described as preparatory (e.g. Weihs, 1973; Domenici and Blake, 1997). However, others have reported significant forces and accelerations of the COM during Stage 1 (reviewed in Wakeling,

2006), the generation of significant force (Borazjani et al., 2012), or the generation of a propulsive jet (Tytell and Lauder, 2008). During the fast start of adult *H. formosa*, the mean effective acceleration of the COM during Stage 1 is significantly larger than 0: on average there is an acceleration component of the COM in the final direction of the escape (Fig. 6). This indicates that, on average, there is already a useful propulsive component of Stage 1, albeit much smaller on average than the propulsive component of Stage 2 (mean effective acceleration: Stage 1, 3.47 m s^{-2}; Stage 2, 15.86 m s^{-2}). Considerable differences occur within this overall pattern, as there is large variation among the analysed fast starts; many have even a negative effective acceleration (Fig. 6). Overall, our results indicate that Stage 1 is always preparatory as the bending of the body aids propulsion in Stage 2, but can have propulsive characteristics of its own in some (but not all) responses.

Determining fast-start performance from an ecological perspective

In this article, we aimed to display the 3D characteristics of the fast-start manoeuvre, i.e. describe its kinematics. However, in an ecological context, the escape performance is relevant for survival, rather than the specific kinematics used during the manoeuvre (Walker et al., 2005). Often in these studies, the performance is described as the instantaneous velocity, total displacement and/or average rotational velocity attained within a given time frame or at a given time point (e.g. Ghalambor et al., 2004; Langerhans, 2009). Similar to measuring at kinematically defined points, fast-start manoeuvres show 3D variability when measured at a fixed time point (Fig. S3). In general, SB responses are slower than DB responses (see also Fig. S1), and would probably result in a reduced survival in case of a predatory strike (Walker et al., 2005).

Fast starts are 3D manoeuvres: implications for related fields

Our observations on the 3D nature of the fast start could aid the understanding of other aspects of the fast-start response. The fast-start response has so far been studied from many different perspectives, including fluid mechanics (e.g. Borazjani et al., 2012; Borazjani, 2013; Li et al., 2014), neurobiology (e.g. Hale, 2002; Canfield, 2006), muscle physiology (e.g. Jayne and Lauder, 1993; Goldbogen et al., 2005), performance-related survival (Walker et al., 2005), and variability of the behaviour (e.g. Marras and Killen, 2011; Jornod and Roche, 2015). However, 3D motion analyses of the body have rarely been published.

To produce 3D motion, 3D forces and moments need to be produced. This is interesting from both a motor control and fluid mechanics point of view, as it requires breaking of dorsoventral symmetry. One mechanism to reach this is by dorsoventrally asymmetric muscle excitation: Nair et al. (2015) postulated that the pitching motion that drives a diving fast start could be the result of inhibition of the motor neurons controlling the epaxial muscles, and excitation of those controlling the hypaxial muscles. This neural signal could span both Stage 1 and Stage 2 in DB starts, explaining the observed sustained pitching motion of the body during these stages (Nair et al., 2015). Work on goldfish has shown that the motion of Stage 2 is irrespective of the motion in Stage 1: Mauthner cells initiate the left–right decision of the escape response during Stage 1 while, simultaneously, parallel circuits control the final escape angle (Eaton et al., 1988). Contrary to the findings of Nair et al. (2015), we find a significant negative relationship between pitch angle changes in Stage 1 and Stage 2. These results indicate that there could be a neural feedback mechanism that controls the amount of pitch depending on the pitch angle change in Stage 1.

A second mechanism to reach dorsoventral asymmetry in forces and moments could incur the use of either set of paired fins. Both pectoral and pelvic fins are known to play a role in changing pitch angles of the body and reducing pitch and yaw instabilities during slow swimming (Lauder et al., 2006; Standen, 2010). Eaton et al. (1977) showed considerable movement of the pectoral fins in hatchetfish, but did not quantify this. The authors described that flexion of the pectoral fins did occur in some instances, simultaneous to the fast body-bend. In knifefish, the pectoral fins were found to be extended throughout the fast-start manoeuvre (Kasapi et al., 1993). The authors speculated that this functioned to increase anterior stability and minimize downward thrust. However, the exact role of the pectoral fins in fast 3D turning is not yet understood. Abduction of the pectoral fin on the inside of the turn could help function as an 'anchor point', and a non-zero angle of attack could induce dorsoventral asymmetry.

Furthermore, the relative vertical displacement during the fast start could change the fluid dynamic effectiveness of the manoeuvre. Pitching motions, for instance, could change how zebrafish larvae interact with their own wake during sharp 'C-bends' (Li et al., 2014). A pitching motion of the head, either upwards or downwards, would alter the 'collision' of the head with the vortex, altering the attained final escape orientation. Simulations need to be performed for a range of naturally occurring body elevations to see if these fast starts are equally effective as fast starts performed in a horizontal plane.

In conclusion, the fast-start escape response is a complex 3D manoeuvre in both larval and adult fish, indicating that the nature of this motion pattern might have been oversimplified in previous studies. This is especially relevant for studies focusing on ecological (survival) parameters of the fast start, as they might be different for planar (horizontal) and 3D motions.

References
Borazjani, I. (2013). The functional role of caudal and anal/dorsal fins during the C-start of a bluegill sunfish. *J. Exp. Biol.* **216**, 1658-1669.

Borazjani, I., Sotiropoulos, F., Tytell, E. D. and Lauder, G. V. (2012). Hydrodynamics of the bluegill sunfish C-start escape response: three-dimensional simulations and comparison with experimental data. *J. Exp. Biol.* **215**, 671-684.

Butail, S. and Paley, D. A. (2012). Three-dimensional reconstruction of the fast-start swimming kinematics of densely schooling fish. *J. R. Soc. Interface* **9**, 77-88.

Canfield, J. G. (2006). Functional evidence for visuospatial coding in the Mauthner neuron. *Brain. Behav. Evol.* **67**, 188-202.

Canfield, J. G. (2007). Some voluntary C-bends may be Mauthner neuron initiated. *J. Comp. Physiol. A Neuroethol. Sensory Neural Behav. Physiol.* **193**, 1055-1064.

Canfield, J. G. and Rose, G. J. (1993). Activation of Mauthner neurons during prey capture. *J. Comp. Physiol. A* **172**, 611-618.

Domenici, P., Blagburn, J. M. and Bacon, J. P. (2011a). Animal escapology I: theoretical issues and emerging trends in escape trajectories. *J. Exp. Biol.* **214**, 2463-2473.

Domenici, P., Blagburn, J. M. and Bacon, J. P. (2011b). Animal escapology II: escape trajectory case studies. *J. Exp. Biol.* **214**, 2474-2494.

Domenici, P. and Blake, R. W. (1991). The kinematics and performance of the escape response in the angelfish (*Pterophyllum eimekei*). *J. Exp. Biol.* **156**, 187-205.

Domenici, P. and Blake, R. W. (1993a). The effect of size on the kinematics and performance of angelfish (*Pterophyllum eimekei*) escape responses. *Can. J. Zool.* **71**, 2319-2326.

Domenici, P. and Blake, R. (1993b). Escape trajectories in angelfish (*Pterophyllum eimekei*). *J. Exp. Biol.* **177**, 253-272.

Domenici, P. and Blake, R. W. (1997). The kinematics and performance of fish fast-start swimming. *J. Exp. Biol.* **200**, 1165-1178.

Domenici, P., Norin, T., Bushnell, P. G., Johansen, J. L., Skov, P. V., Svendsen, M. B. S., Steffensen, J. F. and Abe, A. S. (2014). Fast-starting after a breath: air-breathing motions are kinematically similar to escape responses in the catfish *Hoplosternum littorale*. *Biol. Open* **4**, 79-85.

Eaton, R. C., Bombardieri, R. A. and Meyer, D. L. (1977). The Mauthner-initiated startle response in teleost fish. *J. Exp. Biol.* **66**, 65-81.

Eaton, R. C., DiDomenico, R. and Nissanov, J. (1988). Flexible body dynamics of the goldfish C-start: implications for reticulospinal command mechanisms. *J. Neurosci.* **8**, 2758-2768.

Eilers, P. H. C. (2003). A perfect smoother. *Anal. Chem.* **75**, 3631-3636.

Ellerby, D. J. and Altringham, J. D. (2001). Spatial variation in fast muscle function of the rainbow trout *Oncorhynchus mykiss* during fast-starts and sprinting. *J. Exp. Biol.* **204**, 2239-2250.

Fernald, R. D. (1975). Fast body turns in a cichlid fish. *Nature* **258**, 228-229.

Fisher, N. I. and Lee, A. J. (1982). Nonparametric measures of angular-angular association. *Biometrika* **69**, 315-321.

Fleuren, M., van Leeuwen, J. L., Quicazan-Rubio, E. M., Pieters, R. P. M., Pollux, B. J. A. and Voesenek, C. J. (2018). Data from: Three-dimensional analysis of the fast-start escape response of the least killifish, *Heterandria formosa*. Dryad Digital Repository. https://doi.org/10.5061/dryad.qb5j6

Foreman, M. B. and Eaton, R. C. (1993). The direction change concept for reticulospinal control of goldfish escape. *J. Neurosci.* **13**, 4101-4113.

Ghalambor, C. K., Reznick, D. N. and Walker, J. A. (2004). Constraints on adaptive evolution: the functional trade-off between reproduction and fast-start swimming performance in the Trinidadian guppy (*Poecilia reticulata*). *Am. Nat.* **164**, 38-50.

Goldbogen, J. A., Shadwick, R. E., Fudge, D. S. and Gosline, J. M. (2005). Fast-start muscle dynamics in the rainbow trout *Oncorhynchus mykiss*: phase relationship of white muscle shortening and body curvature. *J. Exp. Biol.* **208**, 929-938.

Hale, M. E. (2002). S- and C-start escape responses of the muskellunge (*Esox masquinongy*) require alternative neuromotor mechanisms. *J. Exp. Biol.* **205**, 2005-2016.

Hedrick, T. L. (2008). Software techniques for two- and three-dimensional kinematic measurements of biological and biomimetic systems. *Bioinspir. Biomim.* **3**, 34001.

Jayne, B. C. and Lauder, G. V. (1993). Red and white muscle activity and kinematics of the escape response of the bluegill sunfish during swimming. *J. Comp. Physiol. A* **173**, 495-508.

Jornod, M. and Roche, D. G. (2015). Inter- vs intra-individual variation and temporal repeatability of escape responses in the coral reef fish *Amblyglyphidodon curacao*. *Biol. Open* **4**, 1395-1399.

Kasapi, M. A., Domenici, P., Blake, R. W. and Harper, D. (1993). The kinematics and performance of escape responses of the knifefish *Xenomystus nigri*. *Can. J. Zool.* **71**, 189-195.

Kawabata, Y., Yamada, H., Sato, T., Kobayashi, M., Okuzawa, K. and Asami, K. (2016). Pelvic fin removal modifies escape trajectory in a teleost fish. *Fish. Sci.* **82**, 85-93.

Kölliker, M. and Richner, H. (2004). Navigation in a cup: chick positioning in great tit, *Parus major*, nests. *Anim. Behav.* **68**, 941-948.

Krupczynski, P. and Schuster, S. (2008). Fruit-catching fish tune their fast starts to compensate for drift. *Curr. Biol.* **18**, 1961-1965.

Langerhans, R. B. (2009). Morphology, performance, fitness: functional insight into a post-Pleistocene radiation of mosquitofish. *Biol. Lett.* **5**, 488-491.

Lauder, G., Madden, P. G. A., Mittal, R., Dong, H. and Bozkurttas, M. (2006). Locomotion with flexible propulsors: I. Experimental analysis of pectoral fin swimming in sunfis. *Bioinspir. Biomim.* **1**, S35-S41.

Lefrançois, C., Shingles, A. and Domenici, P. (2005). The effect of hypoxia on locomotor performance and behaviour during escape in *Liza aurata*. *J. Fish Biol.* **67**, 1711-1729.

Li, G., Müller, U. K., Van Leeuwen, J. L. and Liu, H. (2014). Escape trajectories are deflected when fish larvae intercept their own C-start wake. *J. R. Soc. Interface* **11**, 20140848.

MacRae, P. S. D. and Travis, J. (2014). The contribution of abiotic and biotic factors to spatial and temporal variation in population density of the least killifish, *Heterandria formosa*. *Environ. Biol. Fishes* **97**, 1-12.

Marras, S., Killen, S. S., Claireaux, G., Domenici, P. and McKenzie, D. J. (2011). Behavioural and kinematic components of the fast-start escape response in fish: individual variation and temporal repeatability. *J. Exp. Biol.* **214**, 3102-3110.

Müller, U. K. and Van Leeuwen, J. L. (2004). Swimming of larval zebrafish: ontogeny of body waves and implications for locomotory development. *J. Exp. Biol.* **207**, 853-868.

Nair, A., Azatian, G. and McHenry, M. J. (2015). The kinematics of directional control in the fast start of zebrafish larvae. *J. Exp. Biol.* **218**, 3996-4004.

Singer, J. D. (1998). Using SAS PROC MIXED to fit multilevel models, hierarchical models, and individual growth models. *J. Educ. Behav. Stat.* **23**, 323-355.

Spierts, I. L. Y. and Van Leeuwen, J. L. (1999). Kinematics and muscle dynamics of C- and S-starts of carp (*Cyprinus carpio* L.). *J. Exp. Biol.* **202**, 393-406.

Standen, E. M. (2010). Muscle activity and hydrodynamic function of pelvic fins in trout (*Oncorhynchus mykiss*). *J. Exp. Biol.* **213**, 831-841.

Stewart, W. J., Cardenas, G. S. and McHenry, M. J. (2013). Zebrafish larvae evade predators by sensing water flow. *J. Exp. Biol.* **216**, 388-398.

Tytell, E. D. and Lauder, G. V. (2008). Hydrodynamics of the escape response in bluegill sunfish, *Lepomis macrochirus*. *J. Exp. Biol.* **211**, 3359-3369.

Van Leeuwen, J. L., Voesenek, C. J. and Müller, U. K. (2015). How body torque and Strouhal number change with swimming speed and developmental stage in larval zebrafish. *J. R. Soc. Interface* **12**, 20150479.

Voesenek, C. J., Pieters, R. P. M. and Van Leeuwen, J. L. (2016). Automated reconstruction of three-dimensional fish motion, forces, and torques. *PLoS ONE* **11**, e0146682.

Voesenek, C. J., Muijres, F. T. and van Leeuwen, J. L. (2018). Biomechanics of swimming in developing larval fish. *J. Exp. Biol.* **221**, jeb149583.

Wakeling, J. M. (2006). Fast-start mechanics. In *Fish Biomechanics* (ed. R. E. Shadwick and G. V. Lauder), pp. 333-368. San Diego, CA: Elsevier Academic Press.

Wakeling, J. M. and Johnston, I. A. (1998). Muscle power output limits fast-start performance in fish. *J. Exp. Biol.* **201**, 1505-1526.

Walker, J. A., Ghalambor, C. K., Griset, O. L., McKenney, D. and Reznick, D. N. (2005). Do faster starts increase the probability of evading predators? *Funct. Ecol.* **19**, 808-815.

Webb, P. W. (1976). The effect of size on the fast-start performance of rainbow trout *Salmo cairdneri*, and a consideration of piscivorous predator–prey interactions. *J. Exp. Biol.* **65**, 157-177.

Weihs, D. (1973). The mechanism of rapid starting of slender fish. *Biorheology* **10**, 343-350.

Wöhl, S. and Schuster, S. (2007). The predictive start of hunting archer fish: a flexible and precise motor pattern performed with the kinematics of an escape C-start. *J. Exp. Biol.* **210**, 311-324.
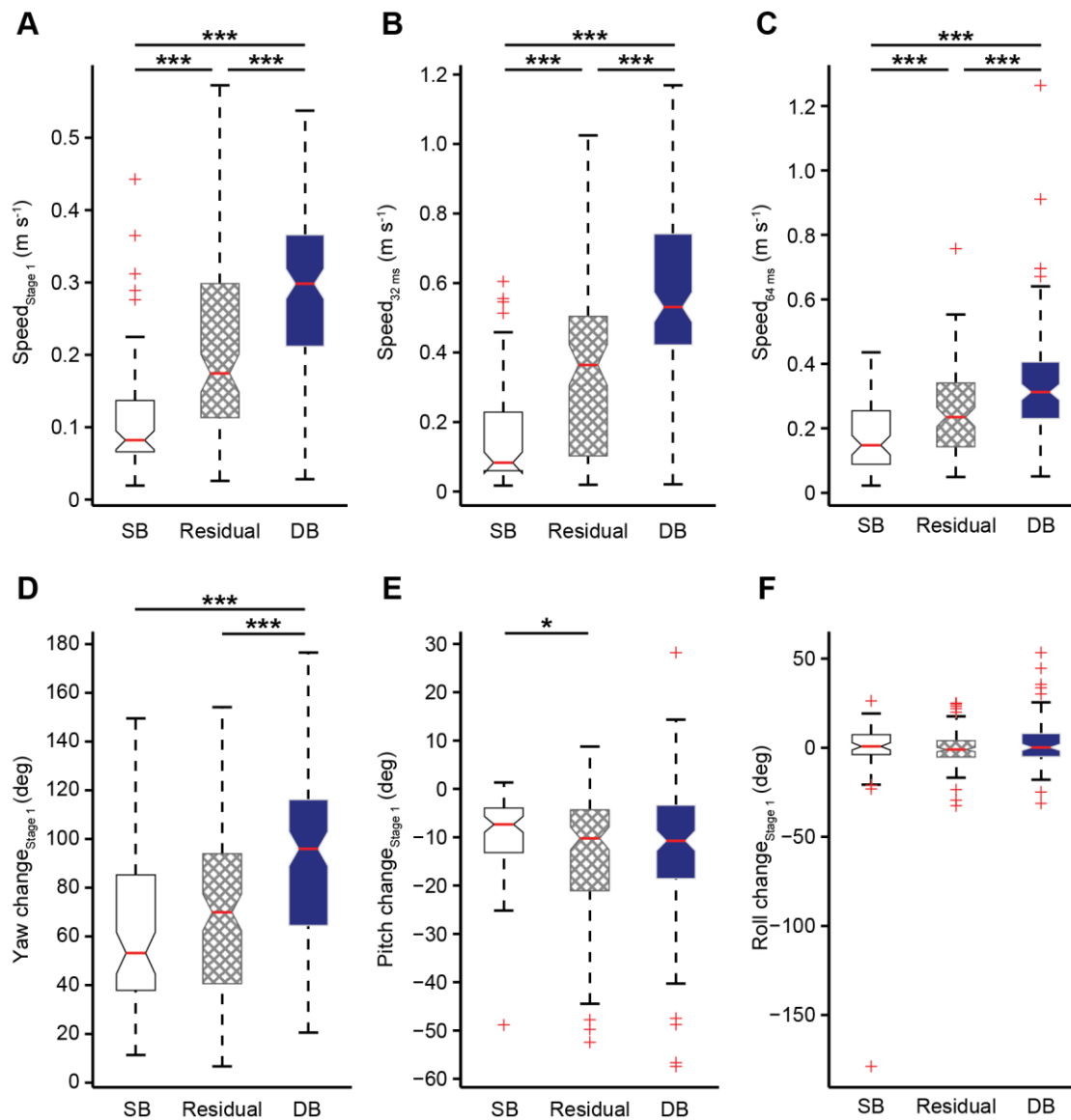
Figure S1: Comparison of single-bend (SB), double-bend (DB) and residual responses for speed and orientation change. N_S = 75 responses, N_D = 133 responses, N_R = 116 responses; from 14 fish. The median is represented by the red lines. Upper and lower edges of the boxes represent 25% and 75% quartiles of the data. Whiskers represent 99.3% of the data, outliers are indicated by red '+'-signs. A: DB responses have a significantly larger speed of the centre of mass (CoM) at the end of Stage 1 (Wilcoxon rank sum test; SB vs. DB − z: -9.6255, $p < .0001$; SB vs. residual − z: -5.8578, $p < .0001$; residual vs. DB − z: -5.6516, $p < .0001$). B: DB responses have a significantly larger speed of the CoM 32 ms after the onset of motion (Wilcoxon rank sum test; SB vs. DB − z: -10.0357, $p < .0001$; SB vs. residual − z: -4.8098, $p < .0001$; residual

vs. DB − z: -6.663, p < .0001). C: DB responses have a significantly larger speed of the CoM 64 ms after the onset of motion (Wilcoxon rank sum test; SB vs. DB − z: -8.0341, p < .0001; SB vs. residual − z: -3.9205, p < .0001; residual vs. DB − z: -4.8966, p < .0001). This time point corresponds with the mean duration until stage 2 for DB responses. D: DB responses have a significantly larger change in yaw angle during Stage 1, while there is no difference between SB and residual manoeuvres (Wilcoxon rank sum test; SB vs. DB − z: -6.0723, p < .0001; SB vs. residual − z: -1.5389, p = 0.1238; residual vs. DB − z: -5.1762, p < .0001). E: There is no significant difference between SB and DB responses in the mean change in pitch angle during Stage 1, but residual manoeuvres have a significantly lower average pitch angle change than SB manoeuvres (Wilcoxon rank sum test; SB vs. DB − z: 1.2668, p = 0.2025; SB vs. residual − z: 2.1219, p = 0.0338; residual vs. DB − z: -1.1423, p = 0.2533). F: There is no significant difference between the response-categories in the mean change in roll angle during Stage 1 (Wilcoxon rank sum test; SB vs. DB − z: 0.3575, p = 0.7207; SB vs. residual − z: 1.6581, p = 0.0973; residual vs. DB − z: -1.3749, p = 0.1692). * 0.05 > p > 0.01; *** p < .0001
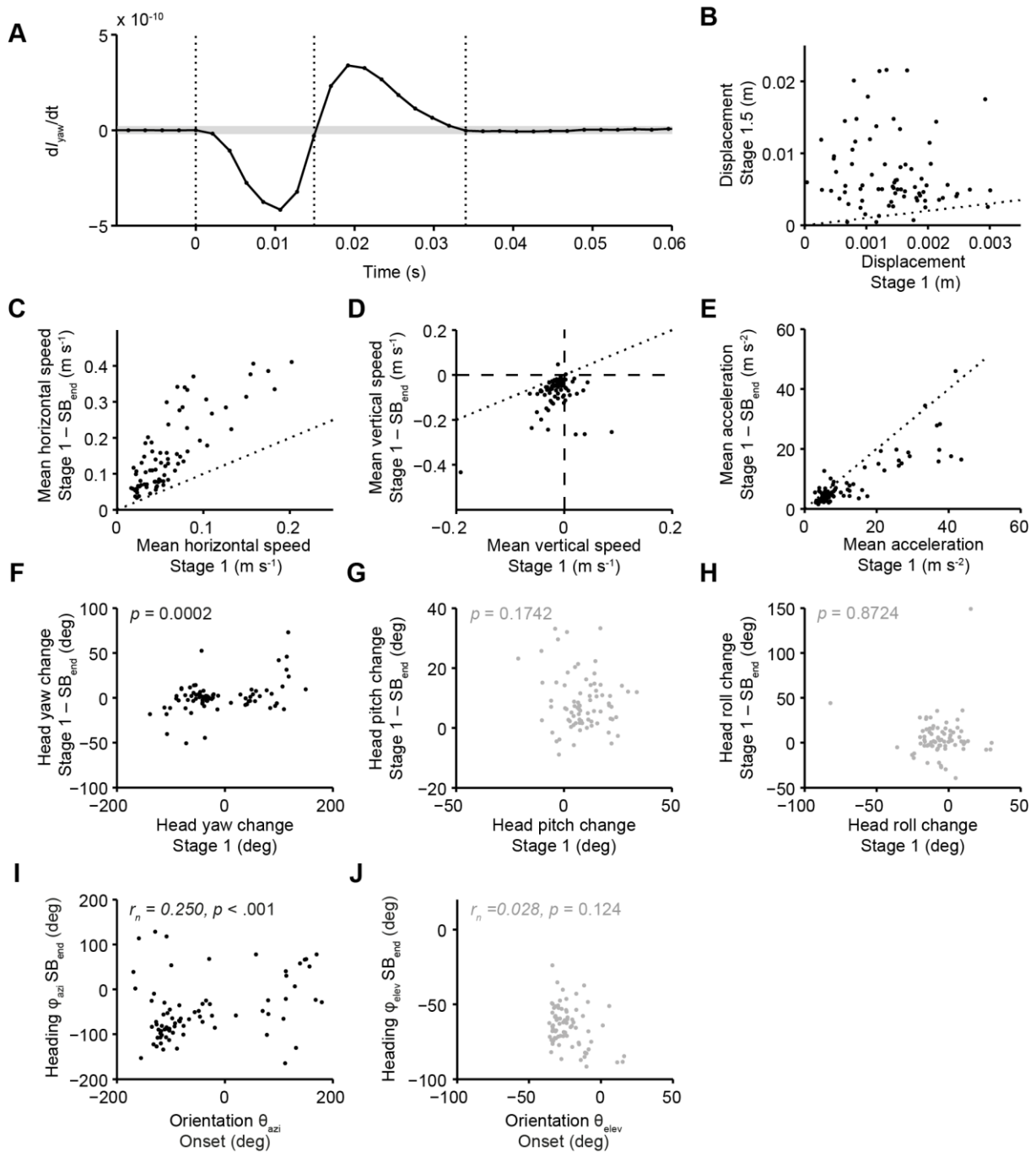
Figure S2: Relationships and correlations between various kinematic performance parameters of Stage 1 and "SB$_{end}$" of single-bend responses. $N_S = 75$ responses, from 14 fish. A: The derivative of the moment of inertia in the yaw plane (I_{yaw}) for a typical single-bend (SB) response. Time is set to 0 s at the onset of motion (the left-most dotted vertical line). The end of Stage 1 is indicated by the second dotted vertical line. The end of SB$_{end}$ (third dotted vertical line) is determined from the first value of dI_{yaw}/dt, following the two peaks, that falls

within a predefined range of values around zero (indicated in grey, see Material & Methods section). B: Displacement of the centre of mass (CoM) during Stage 1 and from the end of Stage 1 until SB$_{end}$. C: Mean horizontal speed of the CoM during Stage 1 and from the end of Stage 1 until SB$_{end}$. D: Mean vertical velocity of the CoM during Stage 1 and from the end of Stage 1 until SB$_{end}$. E: Mean acceleration of the CoM during Stage 1 and from the end of Stage 1 until SB$_{end}$. F–H: Tait-Bryan angle changes during Stage 1 and from the end of Stage 1 until SB$_{end}$; *p*-values are displayed in the top-left corners. F: Yaw-angle changes of the head during Stage 1 and from the end of Stage 1 until SB$_{end}$. G: Pitch angle change of the head during Stage 1 and from the end of Stage 1 until SB$_{end}$. H: Roll angle change of the head during Stage 1 and from the end of Stage 1 until SB$_{end}$. I–J: Correlation between initial orientation of the fish with respect to the stimulus, and escape heading at SB$_{end}$; correlation coefficient *r$_n$* and *p*-values are displayed in the top-left corners. I: Orientation at the onset of motion is correlated with the azimuth heading at the end of the manoeuvre. J: Orientation at the onset of motion is uncorrelated with the elevation heading at the end of the manoeuvre.
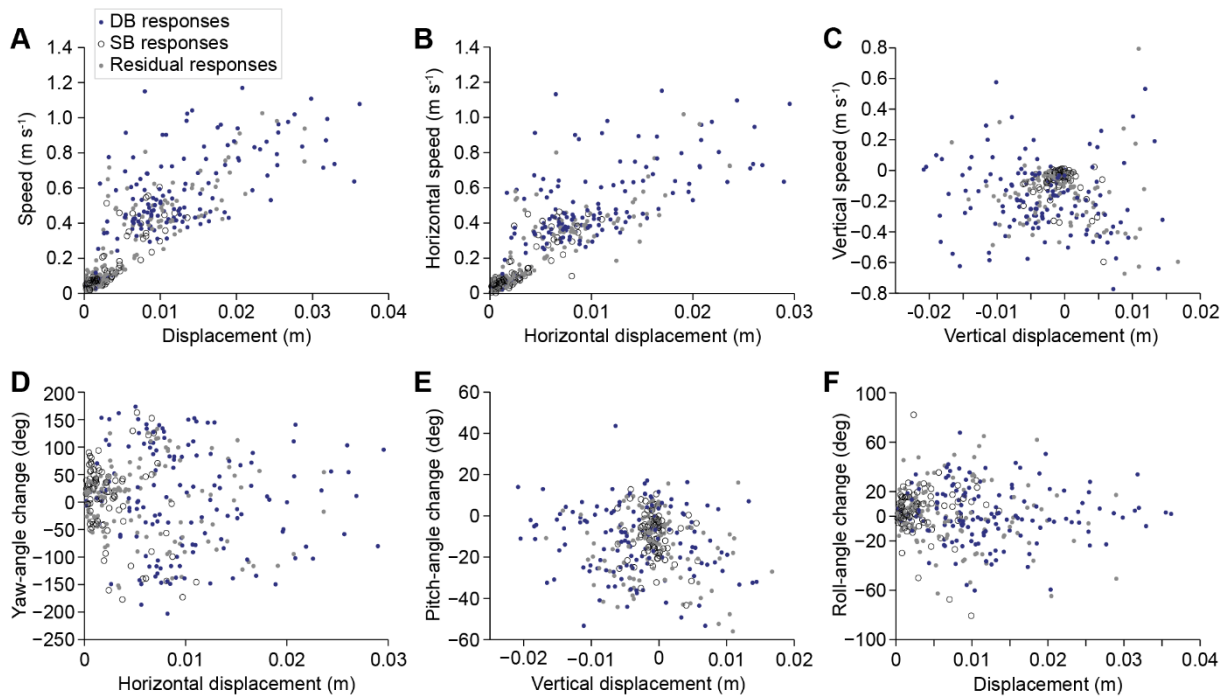
Figure S3: Displacement, velocity and head angle changes at 32 ms after the onset of motion. $N_D = 133$ manoeuvres, $N_S = 75$ manoeuvres, $N_R = 116$ manoeuvres; from 14 individuals. A–C: Scatterplots indicating the relationship between displacement of the CoM in the first 32 ms of the fast-start manoeuvre and its instantaneous speed at 32 ms, split up into combined (A), horizontal (B) and vertical (C) components. D–F: Scatterplots indicating the relationship between displacement of the CoM in the first 32 ms of the fast-start manoeuvre and Tait-Bryan angle changes of the head: yaw (D), pitch (E) and roll (F).

Table S1: Mixed model outputs for correlations between Tait-Bryan angles pitch, yaw and roll of the head in SB starts. All relationships are plotted in Figure S2F–H.

	Model		Intercept (int)			Slope (slp)		
	F	*p*-value	estim.	SE	*p*-value	estim.	SE	*p*-value
Yaw_{head} (1–SB_{end}) = int + slp·Yaw_{head} (O–1)	$F_{1,74}$: 15.15	0.0002	2.3379	1.88	0.2167	0.11	0.03	0.0002
$Pitch_{head}$ (1– SB_{end}) = int + slp·$Pitch_{head}$ (O–1)	$F_{1,73.6}$: 1.88	0.1742						
$Roll_{head}$ (1– SB_{end}) = int + slp·$Roll_{head}$ (O–1)	$F_{1,73.3}$: 0.03	0.8724						

Model: Type 3 test of Fixed Effects

estim: estimates for intercept (int) and slope (slp)

SE: standard errors

Change between time points indicated in brackets. O: onset of motion; 1: end of Stage 1.